arXiv:1611.08101v1 [quant-ph] 24 Nov 2016

Quantum emulation of molecular force fields: A blueprint for a superconducting architecture

Diego G. Olivares,[1] Borja Peropadre,[2,3] Joonsuk Huh,[4] and Juan José García-Ripoll[5]

[1] *Instituto de Física Fundamental IFF-CSIC, Calle Serrano 113b, Madrid E-28006, Spain.*
[2] *Department of Chemistry and Chemical Biology, Harvard University, Cambridge, Massachusetts 02138, United States*
[3] *Quantum Information Processing group, Raytheon BBN Technologies, 10 Moulton Street, Cambridge, Massachusetts 02138, United States*
[4] *Mueunjae Institute for Chemistry, Department of Chemistry, Pohang University of Science and Technology (POSTECH), Pohang 790-784, South Korea.*
[5] *Instituto de Física Fundamental IFF-CSIC, Calle Serrano 113b, E-28006 Madrid, Spain.*

In this work, we propose a flexible architecture of microwave resonators with tuneable couplings to perform quantum simulations of molecular chemistry problems. The architecture builds on the experience of the D-Wave design, working with nearly harmonic circuits instead of with qubits. This architecture, or modifications of it, can be used to emulate molecular processes such as vibronic transitions. Furthermore, we discuss several aspects of these emulations, such as dynamical ranges of the physical parameters, quenching times necessary for diabaticity and finally the possibility of implementing anharmonic corrections to the force fields by exploiting certain nonlinear features of superconducting devices.

I. INTRODUCTION

Among the different controllable quantum systems in the field of quantum technologies, superconducting circuits excel at the possibility of establishing interconnected scalable architectures and tuneable long range couplings. A paradigmatic example of this possibility is the D-Wave architecture [1], in which arrays of superconducting flux qubits are controlled with various parameters: Qubit frequencies, biases, coupling strengths between nearest neighbors and connectivities to other plaquettes [2, 3]. All of these are achieved in a recent implementation of adiabatic quantum optimizers (also known as quantum annealers) [4]. Concerning the architecture, the focus is currently placed on improving the quality of qubits, decreasing their decoherence times and pushing toward larger system sizes.

In this work we explore alternative routes, where the capabilities of D-Wave-type superconducting circuits are leveraged in the context of less demanding applications for quantum simulation. The key idea is that the D-Wave circuit can be moved into a regime in which it behaves as a collection of thousands of resonators with tuneable frequencies, couplings and nonlinearities. It is a powerful platform that can be used to study a wide variety of models. In particular, we show that it can emulate the molecular force fields that govern the vibrational dynamics of complex molecules, with or without anharmonicities.

The typical problem that we have in mind is sketched in Fig. 1, which depicts a molecule that undergoes a change in its force field during an electronic transition. As a consequence of the molecular restructuring, the vibrational modes are displaced, mixed and squeezed through a Duschinsky rotation [5]. Computing the energy distribution for these modes after a sudden change is hard, even more so if anharmonicities are considered.

Here, we show how to map the vibrational structure of a molecule to a superconducting circuit emulator. This map allows to imitate interatomic interactions, emulate sudden, adiabatic or intermediate quenches and experimentally reproduce the Franck-Condon profile (FCP) in the quadratic regime, with the possibility hinted below of including anharmonic corrections to the force field.

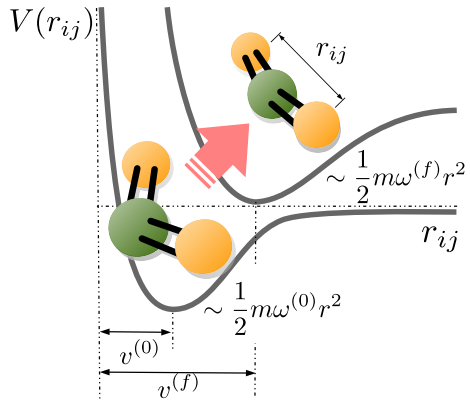

FIG. 1. When a molecule is electronically excited, it feels a sudden change in its force field. This leads to an effective quench and excitation of phonon degrees of freedom. The Franck-Condon profile (FCP) describes the distribution of excitation energies over the vibrational degrees of freedom.

Our proposal is complementary to other applications and proposals for using superconducting circuits to obtain answers to different questions posed in the realm of molecular physics and quantum chemistry [6], such as the study of ground state properties of certain molecules [7] or transport phenomena [8]. It has been already shown that cavity arrays with qubits and boson-sampling techniques [5] can provide information about molecular vibrational spectra and that these may be implemented using

superconducting circuits [9]. We now propose using the same building blocks in a direct implementation of the molecular Hamiltonian, which enables the possibility of taking into account finite quenching speeds (beyond the adiabatic and Franck-Condon approximations), and the effects of other, possibly time-dependent, fields.

This work is structured in three parts. We begin in Sect. II by introducing the particular problem that we intend to emulate: The computation of the FCP [5] that describes the distribution of energies in the vibrational degrees of freedom of a molecule after a sudden quench of its force field. After this, in Sect. III we move on to discuss from a theoretical point of view what operations and protocols are needed to simulate the force field and to reproduce the FCP. We produce mathematically rigorous bounds for a possible physical implementation of the emulator, including preparation, quenching times and measurement protocols. Finally, Sect. IV provides one possible physical implementation of the emulator using a multiply connected architecture of tuneable microwave resonators, together with either some qubits or some microwave detectors. This section leverages on our understanding of such architectures from the realm of circuit-QED and quantum annealers and shows the feasibility of implementing hundreds of vibrational modes together with detailed controls and measurement schemes. We conclude this work with a discussion of possible avenues where these simulators may provide new physical insights, such as the study of nonlinear terms in the molecular force field (see e.g. Ref. [10]), or applications to other computational problems, such as spin models with long-range interactions [11, 12].

II. A MOLECULAR PROBLEM: FRANCK-CONDON PROFILE

When a photoinduced electronic transition takes place in a molecule, the latter experiences vibrational transitions along with the electronic transition (see e.g. Refs. [13–15]). The molecular process is usually described in terms of the Born-Oppenheimer potential energy surface $V(\boldsymbol{x}_1,\ldots,\boldsymbol{x}_N;\Theta)$ of the electronic configuration $|\Theta\rangle$, which is a function of the atomic positions $\{\boldsymbol{x}_i\}$. Here, the state of the molecule is described by a vibronic wavefunction $|\Psi\rangle\otimes|\Theta\rangle$, with separable vibrational ($|\Psi\rangle$) and electronic ($|\Theta\rangle$) components. For a given electronic configuration $|\Theta\rangle$, the atomic dynamics of the molecule can be approximated as a set of coupled harmonic oscillators

$$H_\Theta=\sum_j\frac{1}{2m_j}\,p_j^2+\frac{1}{2}\sum_{jk}\left(\boldsymbol{x}_j-\boldsymbol{v}_j\right)^T A_{jk}^{(\Theta)}\left(\boldsymbol{x}_k-\boldsymbol{v}_k\right). \quad (1)$$

Here, $\boldsymbol{v}$ is the vector of equilibrium positions of the atoms and $A^{(\Theta)}$ is the harmonic force constant matrix (Hessian). m_j and p_j are, respectively, the mass and momentum corresponding to the j-th atom. A Hamiltonian of this form describing the mechanical vibrations of the atoms in a molecule also has an implicit physical symmetry, which is the translational and rotational invariances associated to the rigid motions of the molecule.

With the additional assumption (Condon approximation) of the electronic transition moment $d_{(0,f)}=\langle\Theta_f|\sum_j e\,\boldsymbol{r}_j\,|\Theta_0\rangle$ (where the vectors $\boldsymbol{r}_j$ are the electronic positions) being considered to be independent of the nuclear positions $\boldsymbol{x}_j$, what we are describing here is a sudden electronic transition from an initial vibronic state $|\Psi_0\rangle\otimes|\Theta_0\rangle$ to a final state $|\Psi_f\rangle\otimes|\Theta_f\rangle$. As a consequence of the dipole moment $d_{(0,f)}$ being constant, the transition amplitudes for the nuclear wave function, $\langle\Psi_f|\Psi_0\rangle$, characterize the transition profile.

After the sudden electronic transition, the molecule feels a different force field and undergoes a structural deformation such that the initial wave function $|\Psi_0\rangle$ evolves on a new potential energy surface. Assuming that the final nuclear Hamiltonian H_{Θ_f} can also be approximated by a quadratic interaction Hamiltonian of the form (1), it will also have occupation number eigenstates $|\boldsymbol{n}\rangle$ and eigenenergies $E_{\boldsymbol{n}}=\sum_j\omega_j n_j$. Consequently, the state of the system will evolve as

$$\begin{aligned}|\Psi(t)\rangle&=e^{-i\left(H_{\Theta_f}+E_{\rm el}\right)t}\,|\Psi_0\rangle \\ &=\sum_{\boldsymbol{n}}\langle\boldsymbol{n}|\Psi_0\rangle\,e^{-i(E_{\boldsymbol{n}}+E_{\rm el})t}\,|\boldsymbol{n}\rangle\,,\end{aligned} \quad (2)$$

where $E_{\rm el}$ is the adiabatic electronic transition energy; this off-set energy can be safely set to be zero in our description of the transition probability distribution. The probability distribution $P(E)$ associated to finding the above nonequilibrium states in a given energy manifold is called the Franck-Condon profile (FCP) [16]:

$$P(E)=\sum_{\boldsymbol{n}}\delta\left(E-E_{\boldsymbol{n}}\right)\left\|\langle\boldsymbol{n}|\Psi_0\rangle\right\|^2. \quad (3)$$

The problem of classically reproducing the FCP is linked to two different layers of difficulty. The first one consists in the fact that reconstructing $P(E)$ involves sampling subsets of instances with specific population numbers and it is thereby related to the problem of boson-sampling, which is conjectured to be hard [5, 17, 18]. More precisely, the original boson-sampling problem [19] can appear in the current molecular picture by setting all normal mode frequencies to be approximately the same, preparing the initial Fock states and studying the evolution under an arbitrarily complex change of the force field. The second difficulty lays in the relationship between $P(E)$ and the integer partition problem. Simply put, a given energy $E=\sum_j\omega_j\,n_j$ may be approximated by many different sets of phonon occupation numbers, and reconstructing the full probability distribution involves counting every such possible configuration [5]. Both problems combined make the classical estimation of $P(E)$ arguably hard under general circumstances.

III. QUANTUM EMULATION PROTOCOL

In this section we analyze the steps necessary to implement a complete emulation of the molecular dynamics during a sudden quench of its vibrational structure, followed by a characterization of the resulting states and a computation of the FCP. This is a formal section that introduces the required protocols for the emulation; mathematical operations, preparation, control and measurement of a particular experimental setup and finally interpretation of the results. This discussion sets up the requirements that have to be matched by the physical implementation presented in Sect. IV.

It is convenient for practical reasons to work with Hamiltonians of the form (1) with full-rank coupling matrices $A^{(\Theta)}$. In order to reduce to zero the dimensionality of the kernel of the coupling matrices, which stems from the implicit translational and rotational invariance of $A^{(\Theta)}$, we only need to make the substitution

$$A^{(\Theta)} \;\to\; A^{(\Theta)} + \sum_j \lambda_j^2 \, \boldsymbol{\nu}_j \, \boldsymbol{\nu}_j^T \,, \tag{4}$$

where the quantities λ_j^2 are parameters whose associated frequencies are distinguishable from the physical frequencies of the vibrational model, and the vectors $\{\boldsymbol{\nu}_j\}$ form a basis of its null space. Since the Duschinsky rotations that map different coupling matrices to one another do not affect their kernels, these contributions to the Hamiltonian do not affect the outcome of the experiment, but effectively remove all zero-mode frequencies from the model and stabilize the following protocols and experiments.

Our protocol is defined as a series of prerequisites, some pre-processing phases, some experimental phases and finally a data-gathering phase.

Protocol 1 (Force field approach)**.** *Let us assume a molecular transition* ***problem*** *defined in terms of the following steps:*

1. *a set of oscillator masses, that do not change throughout the experiment, and which form the matrix* $M_{jk} = m_j \, \delta_{jk}$*,*
2. *the initial and final configurations of the vibrational modes defined in terms of the coupling matrices and displacements,* $\left\{A^{(0)}, \boldsymbol{v}^{(0)}\right\}$ *and* $\left\{A^{(f)}, \boldsymbol{v}^{(f)}\right\}$*,*
3. *the eigenfrequencies associated to these models,* $\left\{\omega_n^{(0)}\right\}$ *and* $\left\{\omega_n^{(f)}\right\}$*, upper-bounded by* ω_{max}*,*
4. *and an initial state of the molecule, which may be a thermal or ground state,* $\rho\,(0)$*.*

Let us assume that we have a quantum device, ***the emulator****, described by a set of coupled harmonic oscillators*

$$H_E = \frac{1}{2}\,\boldsymbol{q}^T C^{-1} \boldsymbol{q} + \frac{1}{2}\,\boldsymbol{\phi}^T B\,\boldsymbol{\phi} - \boldsymbol{\phi}^T \boldsymbol{V}, \tag{5}$$

with canonical variables $[\phi_j, q_k] = i\hbar\,\delta_{jk}$*, and with fully adjustable drivings,* V_j*, frequencies and couplings,* $|B_{ij}| \in [\,0,\, B_{max}\,]$*. In comparing Eq. 1 and Eq. 5, we can map the quantum simulation parameters as in the following steps.*

1. *Compute the following auxiliary rescaled matrices and vectors:*

$$B^{(0,f)} = \kappa^2\, C^{1/2} M^{-1/2}\, A^{(0,f)}\, M^{-1/2}\, C^{1/2}\,, \tag{6}$$

$$\boldsymbol{V}^{(0,f)} = \kappa^{3/2}\, C^{1/2} M^{-1/2}\, A^{(0,f)}\, \boldsymbol{v}\,, \tag{7}$$

   with a possible choice $\kappa = B_{max}/\omega_{max}$*.*

2. *Prepare the emulator with the couplings* B *and drivings* $\boldsymbol{V}$ *given by the previous calculation*

$$B_{start} = B^{(0)},\, \boldsymbol{V}_{start} = \boldsymbol{V}^{(0)} - \boldsymbol{V}^{(f)}\,. \tag{8}$$

3. *Prepare the initial state in this emulator, which may be either a ground state (*$|0,\ldots,0\rangle$*) or a (Gaussian) thermal state.*

4. *Suddenly switch, in an appropriate time* T_{sw}*, to the final configuration*

$$B_{end} = B^{(f)},\, \boldsymbol{V}_{end} = 0\,. \tag{9}$$

5. *Measure the* ***total energy*** *stored in the whole resonator array,* E*.*

6. *Based on the previous measurement, gather statistics and reconstruct* $P\,(E)$*, including uncertainties in the estimation of the probability.*

As mentioned before, we will discuss the practical aspects of this protocol in a later section, where we explain how to implement the different steps —for instance model (5) or step 5—, using a particular architecture. Before that, however, we need to explain the theoretical considerations behind the protocol, its steps, and the reasoning behind its design.

1. Model scaling

The first remark is that a molecule and a superconducting emulator do not share the same energy scales: In general, the energies of a superconducting implementation (∼MHz–GHz) will be much smaller than the vibrational energies of a molecule (∼THz or mid-IR). This implies that, for a proper emulation, all the parameters in the Hamiltonian have to be rescaled accordingly in a way that takes into account the allowed frequency ranges of our experiments; both from the point of view of the measurement bandwidth of our emulator, as well as constrained on the temperatures that can be reached in the emulator.

Step 1 of the protocol accomplishes the task of properly designing the emulator parameters in whatever platform

we choose. As discussed in App. A, the transformation in Eq. 6 is an identity that simply changes the length of the canonical variables. This produces a Hamiltonian whose physics is similar, but in which the frequencies have been rescaled from ω_n to $\Omega_n = \kappa\,\omega_n$. All the other observables may be similarly reconstructed:

$$\text{Molecule} \leftrightarrow \text{Emulator}$$
$$\boldsymbol{p} = \frac{1}{\sqrt{\kappa}}\, M^{1/2}\, C^{-1/2}\, \boldsymbol{q}\,, \tag{10}$$
$$\boldsymbol{x} = \sqrt{\kappa}\, M^{-1/2}\, C^{1/2}\, \boldsymbol{\phi}\,.$$

Finally, it is important to clarify that the choice of scaling in Step 1 is not unique. There may be others that are motivated not by the size of couplings but by maximum achievable frequencies, setup constraints, etc.

2. Independent resonators and measurement

The final remark is that we have engineered Steps 3 to 4 in Protocol 1 as moving from generic initial (B_{start}) to final (B_{end}) coupling matrices, and finally measuring the total power in the resonator array. This is indeed possible, as we argue below in Sect. IV, yet in many circumstances it would be more advantageous to end up at a configuration such that every normal mode is associated to an *independent resonator* through its variables $\{q_j, \phi_j\}$. This is a particularly easy thing to accomplish when the "mass" matrix C in the emulator (5) is diagonal. If this is achieved, we can provide means to inquire the populations of these independent resonators individually —for instance, by coupling qubits or other detectors to each resonator, as illustrated in Fig. 2—; thereby obtaining even more information than just the FCP, such as entanglement and correlations between modes, or full Wigner function representations.

These techniques are discussed in Sect. IV D, requiring only a slight modification of the protocol.

Protocol 2 (Normal mode approach)**.** *This protocol reproduces the assumptions and steps in Protocol 1, but replaces the following steps:*

1'. Compute the following auxiliary rescaled matrices and vectors:

$$B^{(0,f)} = \kappa^2\, C^{1/2} M^{-1/2}\, A^{(0,f)}\, M^{-1/2}\, C^{1/2}\,, \tag{11}$$
$$\boldsymbol{V}^{(0,f)} = \kappa^{3/2}\, C^{1/2} M^{-1/2}\, A^{(0,f)}\, \boldsymbol{v}\,, \tag{12}$$

with a possible choice $\kappa = \Omega_{max}/\omega_{max}$.

Diagonalize the target configuration $B^{(f)} = O\,\Omega^{(f)}\,O^T$ in order to find the final rescaled eigenfrequencies, $\Omega_j^{(f)} = \kappa\,\omega_j^{(f)}$ and orthogonal transformation O.

2'. Prepare the emulator with the paramters

$$B_{start} = O^T B^{(0)} O,\; \boldsymbol{V}_{start} = O^T \left(\boldsymbol{V}^{(0)} - \boldsymbol{V}^{(f)}\right). \tag{13}$$

4'. Suddenly switch, at an appropriate time T_{sw}, to the final configuration of uncoupled resonators

$$B_{end} = \Omega^{(f)},\; \boldsymbol{V}_{end} = 0\,. \tag{14}$$

*5'. Measure the **number of phonons** in each of the decoupled resonators, n_j, and reconstruct the energy*

$$E = \sum \omega_j^f\, n_j\,. \tag{15}$$

3. Quench times and errors

The second remark is that Step 4 need not be "instantaneous" to succeed —indeed, there exists nothing instantaneous in real experimental setups, and real quenches always involve a finite amount of time T_{sw} [cf. Sect. IV B]. Fortunately, we can approximately solve the dynamics of the emulator state during the quench time. Using time-dependent perturbation theory, we prove analytically in App. B that there exists an upper bound to T_{sw} such that any quench faster than this time will produce a final state approximately unperturbed and as close to the ideal case $T_{\text{sw}} \to 0$ as we wish.

To be more precise, we have proven the following:

Proposition 1. *If we adjust the quench time as*

$$T_{sw} = \epsilon \times \mathcal{O}\left(\min\left\{\frac{1}{\Omega_{max}}, \frac{2}{\|C^{-1/2}\,\boldsymbol{V}_{start}\|}\right\}\right), \tag{16}$$

the final state will approximate to the ideal quench ($T_{sw} \to 0$) with small errors $\mathcal{O}(\epsilon)$, in (i) the first and second moments, (ii) the total energy of the final state and (iii) the fidelity of the state.

Notice that the switching is not only constrained by the fastest timescale in the Hamiltonian, but also that it depends on the initial displacement of the vibrational modes. The intuition is that, when the minima of the initial and final configurations are far apart from each other, the Wigner function of the quenched state will start far away from the origin and it will change very rapidly in phase space, with a velocity $\sim$ displacement $\times\,\omega$. In order to avoid any relevant change in the quantum state during the quench time we need that T_{sw} scales as the inverse of the average number of photons stored in the resonator in the quenched state, which is the physical interpretation of $\left\| C^{-1/2}\,\boldsymbol{V}_{\text{start}}\right\|$. This is the reason why the null space is forcibly removed from beforehand in (4): Modes in the null space of the vibrational Hamiltonian, which correspond to the rigid degrees of freedom (translational and rotational) of the molecule, would have a marginally low frequency in a realistic emulation on a superconducting architecture. As a consequence, these modes could host a large population of photons. This is undesirable as it would decrease the switching times T_{sw} necessary to approach the ideal quench, as these photons could leak into the cavities that represent vibrational modes through imperfections in the switching off of the tuneable couplings.

IV. PHYSICAL IMPLEMENTATION

So far, we have introduced the emulation protocol in a formal way. We will now discuss how every stage of the emulation, from the initial preparation to the final measurement, can be implemented by using superconducting circuits.

A. Tuneable resonator array

The basic ingredient in our emulation protocol is the possibility of implementing the model (5) with tuneable parameters B and $\boldsymbol{V}$. Our suggestion consists in using superconducting microwave resonators for this task. A possible architecture for such ensemble of resonators is shown in Fig. 2, where we graphically intertwine 9 tuneable resonators that cross over each other. Note that these resonators interact with each other at their crossing points either directly or through circuits implementing an adjustable mutual inductance.

There exist multiple proposals for implementing both tuneable resonators and tuneable couplings between them, which rely on different variations of SQUIDs both for the tuning [20, 21] and the coupling [22]. We believe, however, that a promising approach is to revisit the D-Wave architecture of flux qubits to implement this type of setups. In particular, D-Wave qubits, when brought back close to zero flux bias, are nothing but tuneable SQUIDs in which the plasma frequency can be adjusted with external magnetic fields. Moreover, there exist robust variations of the SQUID setup that have been proposed and tested with such qubits [2, 3], both for the purposes of tuning frequencies and couplings. In contrast with the qubit regime, our demands for fidelity and dephasing are much more relaxed. The need for less coupled elements, as well as ongoing progress in the design of controls for superconducting circuits, may significantly improve the switching times for frequency and coupling, which in the D-Wave architecture were very long.

Irrespectively of the architecture that is finally used, the effective lumped element circuit of the resonator array can always be written in the linear form as

$$H = \frac{1}{2}\,\boldsymbol{q}^T C^{-1}\,\boldsymbol{q} + \frac{1}{2}\,\boldsymbol{\phi}^T L^{-1}\,\boldsymbol{\phi} + \boldsymbol{\phi}^T L_{\rm ext}^{-1}\,\boldsymbol{\phi}_{\rm ext}\,, \qquad (17)$$

where C and L are respectively the capacitance and inductance matrices, and the last term is the inductive energy associated to the coupling with external currents. The terms in the matrix C come from the local capacitance of each resonator, C_{jj}, as well as the mutual capacitance to its neighbors, $C_{j\neq k} \ll C_{jj}$. The inductance matrix contains both the diagonal terms that we use to control the frequency of each resonators, $(L^{-1})_{jj}$, as well as the mutual inductance between different resonators, $(L^{-1})_{j\neq k}$.

In this setup, the matrices C, L and the vector $\boldsymbol{I} = L_{\rm ext}^{-1}\,\boldsymbol{\phi}_{\rm ext}$ map directly to the equivalent objects C, B and $\boldsymbol{V}$ in Eq. 5. All the inductive elements, L, and currents, $\boldsymbol{I}$, are susceptible of external control when we place tuneable elements, such as SQUIDs, either on the resonators or the intersections [cf. Fig. 2]. By using these elements, we can prepare the desired matrix $B \sim L^{-1}$ and driving $\boldsymbol{V}$, both before and after the quench.

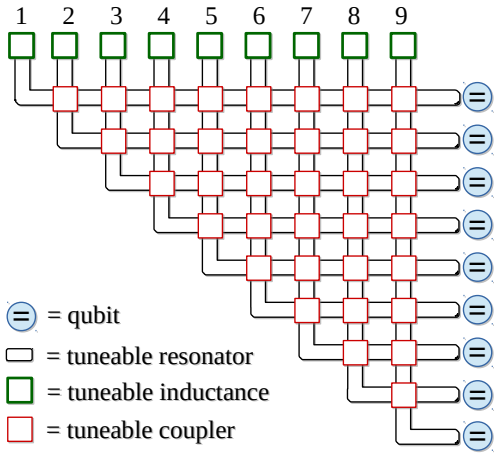

FIG. 2. Schematic representation of a scalable architecture of superconducting resonators (black tubes) connected by tuneable interactions at their intersections (red boxes), and with tuneable inductors to change their frequency (top boxes). Each resonator may or may not be coupled to an additional qubit (circle) for preparation and measurement purposes.

Note that our formalism for the quenches considers the possibility of having a capacitance matrix with non-local interactions, $(C^{-1})_{jk} \neq 0$. As it was discussed before, the only moment at which this matters is at the final stages of Protocol 2, when we attempt to make the matrix $B_{\rm final}$ almost diagonal [cf. Step 4']. If C^{-1} is almost diagonal too, it turns out that we have N truly decoupled resonators that can be measured independently using the variant of Step 5'. However, if there is a residual mutual capacitance $C_{j\neq k}$, the final resonators will be weakly coupled, and there is a possibility of cross-talk, for instance, when we place qubits close to resonance to measure the number of photons [cf. Fig. 2]. Such an effect can be remedied by choosing a different $B_{\rm final}$ that truly makes the oscillators decouple while the desired final frequencies are preserved.

B. Parameters, frequencies and drivings

As was mentioned in the prerequisites of the protocol, we have to take into account the fact that we may not implement arbitrarily large or small resonator frequencies. In practice, the emulator will work with a spectrum of harmonic eigenfrequencies that will be rescaled with respect to the molecular eigenenergies

$$\Omega_n^{(0,f)} = \kappa \times \omega_n^{(0,f)}\,. \qquad (18)$$

We have to design our emulator scaling κ such that the values Ω_n fit within experimental constraints. For instance, the lower frequency limit is typically imposed by the temperature of the superconducting chip, which will be of the order of tens of mK. This means that ideally $\Omega_n \geq \Omega_{\min} \sim 200$ MHz. The upper bound, on the other hand, is given by the bandwidth of our measurement devices, so that we can reasonably assume $\Omega_n \leq \Omega_{\max} \sim 20$ GHz for a state-of-the-art experiment. In this case, to ensure diabaticity we have to expect that the switching of coupling and frequencies takes place at a rate $1/T_{\rm sw} \gg 20$ GHz, which seems a feasible figure as shown by circuit QED experiments [20].

Once the range of allowed frequencies is known, we have to adjust the experimental parameters to fit within this region. Considering the pair of coupling matrices $A^{(0)}$ and $A^{(f)}$ which are going to be implemented during a simulation, we extract their associated spectra, $\{\omega_n^{(0,f)}\}$. We may now simply take $\omega_{\max} = \max\left(\{\omega_n^{(0,f)}\}\right)$ and apply a frequency rescaling

$$\kappa = \Omega_{\max}/\omega_{\max}\,. \tag{19}$$

Using this scaling we have a dynamical range

$$\frac{\omega_{\max}}{\omega_{\min}} < \frac{\Omega_{\max}}{\Omega_{\min}} \sim 100\,, \tag{20}$$

which is sufficient for most molecules, and which safely lays within the working conditions of most experiments with superconducting circuits.

The λ_j parameters introduced in (4) to prevent an overpopulation of photons in modes of marginally low frequency (as was discussed at the end of Sec. III 3) have to be chosen in such a way that, after the rescaling, their frequencies lie in this dynamical range and are distinguishable from the frequencies associated to physical vibrational modes.

C. State preparation

If the resonator frequencies are engineered according to the requirements laid out in the previous subsection, it will be possible to prepare the initial state of the resonators in an almost zero-temperature state. This can be achieved by simply waiting for a sufficiently long time until the temperature given by the cryostat sinks into the circuit. At temperatures $T_{\rm cryo} < \hbar\Omega_{\min}/K_{\rm B}$, the number of photonic excitations will be negligible. Microwave-induced cooling techniques [23, 24] may also be considered in the case of low frequencies lying below the cryostatic range.

Should we wish to prepare a thermal state, it can also be achieved in two possible ways. One is to lower the frequencies of the array so that the effective temperature of the cryostat populates the resonator. In other words, we choose κ differently, so that

$$\kappa = \frac{T_{\rm molecule}}{T_{\rm cryo}} \;\Leftrightarrow\; \frac{\hbar\Omega_0}{K_{\rm B}T_{\rm cryo}} = \frac{\hbar\omega_0}{K_{\rm B}T_{\rm molecule}}\,. \tag{21}$$

The other possibility is to couple the resonator array to a source of incoherent microwave radiation with a thermal distribution at the desired effective temperature. Such drivings, which can be obtained from simple resistances, have been already demonstrated in the literature and are routinely used for calibrating tomographic setups for quantum microwaves [25, 26].

D. Measurement

The final point of the protocol, after having performed an emulation of the quenching transition, is extracting information that allows us reconstructing the FCP, using the superconducting cavities that emulate the vibrational modes. A variety of strategies may be used for the measurement stages, depending on the physical observables that we intend to characterize.

The simplest approach towards measuring the total energy of the resonator array would be to study the power that is leaked out from the resonators. By coupling each resonator to a transmission line, we can extract the outgoing microwaves, add them up and, after amplification, measure the total radiated power in an integrating device. The resulting measure of the leaked intensity will be proportional to the number of photons in the resonator and their respective energies, as per the input-output relations. These measurements will provide us with a power distribution $P(W)$ which we can assimilate to the FCP $P(E)$ after a suitable calibration. The contributions on the rescaled λ_j parameters corresponding to the null space of the coupling matrices have to be substracted to assimilate the power distribution to the FCP.

This is not the only possibility, as actual setups may have amplifiers which are noisier or are too narrow-bandwidth. In that case, it may be more desirable to measure the number of photons directly in each resonator, or the collective energy of the setup, using one of the schemes we suggest in App. C.

V. ANHARMONICITY

One of the most interesting features of the superconducting architecture is the possibility of emulating molecular systems with full control of the nonlinear terms. As sketched in Fig. 1, general force field potentials are not exactly harmonic near their global minima. A better approximation would be a quartic Taylor expansion around the minimum

$$V(x_0+\delta x) \simeq c_2\,\delta x^2 + c_3\,\delta x^3 + c_4\,\delta x^4 + \mathcal{O}\left(\delta x^5\right), \tag{22}$$

where $c_n = \partial_x^n V(x_0)/n!$. Introducing cubic or quartic terms in classical simulations of molecular quenches is extremely difficult, with molecules with a small number of components exhausting computational capabilities. This happens because the states involved are no longer Gaussian and cannot be efficiently approximated by a first-

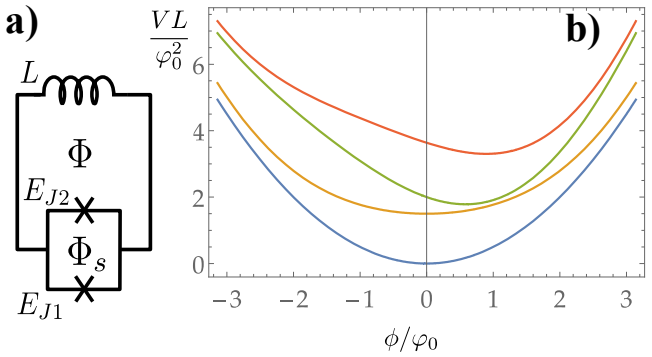

FIG. 3. (a) Superconducting circuit formed by a couple of Josephson junctions in a SQUID configuration and an associated linear inductance. (b) Energy curves of the circuit potential in Eq. 23, for $(L/L_J, \Phi/\varphi_0) = (0,0)\,,\ (0.5,0)\,,\ (0.7,-\pi/2)$ and $(0.9,-\pi/4)$, from bottom to top. Curves have been shifted arbitrarily upwards for better visibility.

and second-order moments (see e.g. Ref. [10]). However, adding such nonlinearities to the superconducting setup from Fig. 2 is rather straightforward and should be the subject of future work.

As an example, in this section we discuss how replacing a simple LC-resonator with the SQUID setup in Fig. 3 allows us to achieve any effective nonlinearity with reasonable parameters. We will work with the inductive energy around the minimum of

$$V(\phi) = E_J(\Phi_s)\cos\left[(\phi-\Phi)/\varphi_0\right] + \frac{1}{2L}\phi^2\,, \tag{23}$$

which contains the static contribution of the linear inductor, L, the effective Josephson energy of the SQUID, E_J, and the external fluxes trapped in the loops, Φ_s and Φ. In order to prove *universality* up to fourth order, we only have to find the energy minima of $V(\phi)$ and verify that it can be expanded as Eq. 22 with any possible ratio of c_3/c_2 and c_4/c_2. To do this, we can focus on the limit in which the parabolic term $\phi^2/2L$ is the dominant contribution, as this can always be achieved replacing the inductor with a larger junction. The minimal energy configurations may be then obtained by expanding around $\phi = 0$, which yields the solution $\phi_{\min} \simeq \Phi/(1+L_J/L)$, where $L_J(\Phi_s) = \varphi_0^2/E_J(\Phi_s)$ is the effective Josephson inductance. Notice that the Taylor expansions around the energy minimum starts at the second order, with $\partial_\phi^2 V \sim 1/L$. The cubic and cuartic corrections are also found to be

$$\frac{c_3}{c_2} \simeq \frac{1}{1+L_J/L}\,\frac{\Phi}{\varphi_0^2}\,, \tag{24}$$

$$\frac{c_4}{c_2} \simeq -\frac{L}{L_J}\,\frac{1}{\varphi_0^2}\,. \tag{25}$$

Since $L_J \propto \cos(\Phi_s)$ can be changed in sign and magnitude independent of Φ, we have that c_3/c_2 and c_4/c_2 may be tuned separately in order to approximate anharmonic potentials up to $\mathcal{O}(\phi-\phi_{\min})^5$.

The flexibility of this circuit is exemplified in Fig. 3 for different values of the SQUID inductance and inner flux. For $\Phi = 0$ and $L/L_J = 0$, the model is basically harmonic, and the circuit may be used as a tuneable resonator. However, as we increase the strength of the SQUID, ϕ^4 terms become dominant, and the potential can become asymmetric, in closer resemblance with usual Morse potentials.

This idea of anharmonic oscillators can be extended to a multi-mode circuit and also to the coupling terms between different variables in Eq. (5). While scaling up this design to many modes becomes complicated and requires a careful crafting of the different fluxes, the fact is that, as we mentioned before, already a single-purpose emulator capable of reproducing molecules with a few anharmonic modes would surpass the computational capabilities of existing classical algorithms.

As for the other considerations in this work, the addition of weak anharmonicities does not significantly modify the discussion on the quench times or the measurements. In the first case, we might have to verify that the quench time is shorter than the inverse of the anharmonic terms, $T_{\rm sw} < 1/c_n \left\|C^{-1/2}\,\boldsymbol{V}\right\|^{n/2}$, extending the previous bounds. However, as in general $c_{3,4} \gg c_2$ we expect that the introduction of nonlinearities will not impose further constraints in the quench dynamics. In the case of the measurements, we can still rely on the leakage from the oscillators for measuring power. If this is not possible or desirable for a given setup, we may always resort to spectroscopic means to interrogate the resonator energies, as described in App. C.

VI. OUTLOOK AND CONCLUSIONS

In summary, we have provided a full framework for the quantum emulation of a molecular force field using an array of tuneable microwave resonators which leverages the D-Wave design [cf. Fig. 2]. We have derived precise protocols for gathering information about molecular transitions and in particular the Franck-Condon spectra using such platform, including a detailed discussion of all steps, from the tuning of the emulator to the measurement phase. Finally, we have provided evidence that this architecture, when working in anharmonic regimes, may be even more useful and surpass the capabilities of existing classical algorithms.

As a practical example of the application of this emulation framework, we present the case of a vibronic transition between two different vibrational configurations the formic acid molecule (HCOOH) and how the parameters to emulate a vibronic transition in a superconducting architecture may be picked. The data for the force constants $A_{jk}^{(0,f)}$ and atomic positions $|\delta\boldsymbol{v}_j|$ in both of the configurations considered have been extracted from Ref. [16]. Every physical parameter that characterizes both harmonic models (1) for two different vibrational

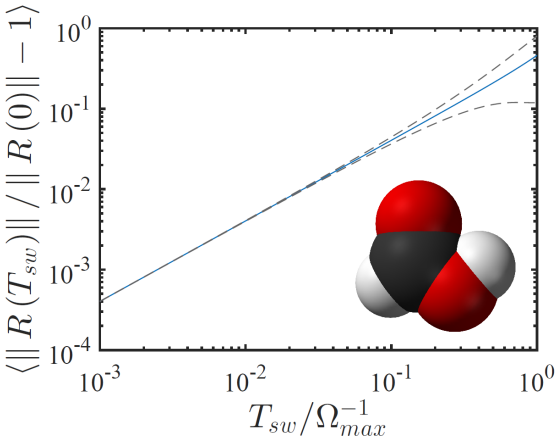

FIG. 4. Scaling of vector norm differences during a quenching of duration T_{sw} in the formic acid molecule, estimated from the exact time evolution of the system described by Hamilton's equations from a complete and orthogonal set of initial conditions. It is observed that the mean value of these differences (solid line) increases linearly with T_{sw}, which is consistent with the obtained bounds [cf. App. B]. The variance from the mean of this set of norm differences (dashed lines) is shown around the mean value, and is found to be small for short times $T_{sw}\Omega_{max} \ll 1$.

configurations of this molecule finds its respective counterpart in the superconducting emulator scheme (5):

Molecular parameters		Superconducting emulator	
M_{jj}	1–16 a.m.u.	0.5–8 pF	C_{jj}
$A_{jk}^{(0,f)}$	$6.1 \cdot 10^{-3}$–101 eV/Å^2	$2.37 \cdot 10^{-4}$–3.83 nH^{-1}	$B_{jk}^{(0,f)}$
$\hbar\omega_j$	62–467 meV	1.33–10 GHz	$\Omega_j/2\pi$
$\lvert\delta v_j\rvert$	0.32–7.8 pm	1.27–116 nA	$\lvert\delta V_j\rvert$

These parameters have been obtained by choosing a maximum working frequency for the resonators in the emulator of 10 GHz, which determines the frequency rescaling factor $\kappa = \Omega_{\max}/\omega_{\max}$, and a choice of cavity capacitances consistent with the atomic masses in the molecule. The mutual inductances B_{jk} and drivings $\boldsymbol{V}_j$ can be obtained from these previous parameters and the formic acid parameters using (6) and (7).

In order to reproduce the FCP, the quenching time $T_{\rm sw}$ between the two different oscillatory configurations has to be short enough so that the Franck-Condon approximation [cf. Sec. II] still applies. As discussed in Sec. III 3, the state of the system should remain unaffected at the end of quench if $T_{\rm sw}$ is shorter than the bound (16), which only depends on parameters of the emulation.

We backup the aforementioned discussion with numerical simulations for different switching times of a realistic quenching process between these two vibrational configurations of the formic acid molecule. In the simulations, we have reproduced a quench between the two different quadratic models considered (that we call here H_1 and H_2), using a linear switching profile $H(t) = (1 - t/T_{\rm sw})\, H_1 + t/T_{\rm sw}\, H_2$. Picking a complete and orthogonal set of initial conditions for the atomic positions and momenta, we have run simulations of the time evolution of the system as governed by Hamilton's equations. The observed changes in the vector norms shown in Fig. 4 are small enough and scale linearly with $T_{\rm sw}\Omega_{\max}$ [cf. App. B], so the deviation from the original state of the system may be bounded as stated in Proposition 1.

Our work is an example of another family of useful problems that can be implemented in a superconducting circuit setup. It would be experimentally relevant and interesting to pursue the design of single-purpose circuits for highly anharmonic molecules with few atoms. Existing blueprints for the D-Wave architecture, as well as ongoing efforts for higher-fidelity quantum annealers with flux qubits could be leveraged for this task.

ACKNOWLEDGMENTS

This work has been funded by MINECO Project FIS2015-70856-P and CAM Research Network QUITEMAD+. D.G.O. acknowledges support from MINECO by FPI grant BES-2013-066486. B.P. acknowledges the Air Force of Scientific Research for support under award: FA9550-12-1-0046. J.H. acknowledges supports by Basic Science Research Program through the National Research Foundation of Korea (NRF-2015R1A6A3A04059773) and Mueunjae Institute for Chemistry (MIC) postdoctoral fellowship.

Appendix A: Rescaling of Hamiltonians

Let us assume we want to simulate a harmonic model

$$H = \frac{1}{2}\,\boldsymbol{p}^T M^{-1}\boldsymbol{p} + \frac{1}{2}\,(\boldsymbol{x}-\boldsymbol{v})^T\, A_{ij}\,(\boldsymbol{x}-\boldsymbol{v})\,, \qquad \text{(A1)}$$

with canonical variables $[x_i, p_j] = i\hbar\,\delta_{ij}$, using a family of tuneable Hamiltonians

$$H_E = \frac{1}{2}\,\boldsymbol{q}^T C^{-1}\boldsymbol{q} + \frac{1}{2}\,\boldsymbol{\phi}^T B\,\boldsymbol{\phi} - \boldsymbol{\phi}^T\,\boldsymbol{V}\,, \qquad \text{(A2)}$$

with other canonical variables, $[\phi_i, q_j] = i\hbar\,\delta_{ij}$, and different energy scales. We will show that both models can be mapped to each other through a suitable change of scales. For that let us write down the transformation

$$\boldsymbol{q} = U^T\boldsymbol{p}, \quad \boldsymbol{\phi} = U^{-1}\boldsymbol{x}\,, \qquad \text{(A3)}$$

which preserves the commutation relations

$$[\phi_i, q_j] = \sum_{m,n} \left(U^{-1}\right)_{im} U_{nj}\,[x_m, p_n] = i\hbar\,\delta_{ij}\,. \qquad \text{(A4)}$$

This leads to the model

$$H_E = \frac{1}{2}\,\boldsymbol{p}^T U\, C^{-1} U^T\boldsymbol{p} + \frac{1}{2}\,\boldsymbol{\phi}^T\left(U^{-1}\right)^T B\, U^{-1}\boldsymbol{\phi} + \\ - \boldsymbol{x}^T\left(U^{-1}\right)^T\,\boldsymbol{V}\,. \qquad \text{(A5)}$$

In order for H and H_E to be equivalent, we just need $H_E = \kappa H + E_0$, with some constants κ and E_0. This assumption leads to the condition

$$\kappa\, M^{-1} = U\, C^{-1} U^T,\, B = \kappa\, U^T A\, U,\, \boldsymbol{V} = \kappa\, U^T A\, \boldsymbol{v}\,. \tag{A6}$$

Using the fact that C and M are symmetric matrices we deduce

$$U^T = \sqrt{\kappa}\, C^{1/2} M^{-1/2}, \quad \left(U^{-1}\right)^T = \frac{M^{1/2}\, C^{-1/2}}{\sqrt{\kappa}}\,, \tag{A7}$$

$$U = \sqrt{\kappa}\, M^{-1/2} C^{1/2}, \qquad U^{-1} = \frac{C^{-1/2}\, M^{1/2}}{\sqrt{\kappa}}\,. \tag{A8}$$

and obtain the suitable oscillator parameters

$$B = \kappa^2\, C^{1/2} M^{-1/2} A\, M^{-1/2} C^{1/2}, \tag{A9}$$

$$\boldsymbol{V} = \kappa^{3/2}\, C^{1/2} M^{-1/2} A\, \boldsymbol{v}. \tag{A10}$$

At this point we have an absolute freedom to choose κ. We can select

$$\kappa = \frac{B_{\max}}{\omega_{\max}}\,, \tag{A11}$$

where $\omega_{\max}$ is the largest eigenfrequency of the normal modes in H, and $B_{\max}$ is the largest dynamical range of the eigenfrequencies and couplings in B, that is, $B_{\max} = \max_{kl} |B_{kl}|$. We assume that there are no restrictions in the strength of V.

Finally, notice that the mapping of Hamiltonians is accompanied by a mapping of physical observables, which becomes Eq. (10) once our choice of U is made.

Appendix B: Switching times and diabatic condition

We can give an upper bound to the time $T_{\rm sw}$ required to switch Hamiltonians and still preserve the state of the system (2) with sufficient fidelity. Without loss of generality, we assume a linear interpolation between the initial and final sets of couplings, which translates into a linear interpolation between Hamiltonians

$$\begin{aligned} H_E\,(t) =& \left(1 - \frac{t}{T_{\rm sw}}\right) H_{\rm E,start} + \frac{t}{T_{\rm sw}}\, H_{\rm E,final} \\ =& \frac{1}{2}\, \boldsymbol{q}^T C^{-1} \boldsymbol{q} + \frac{t}{T_{\rm sw}}\, \boldsymbol{\phi}^T B_{\rm final}\, \boldsymbol{\phi} + \\ &+ \left(1 - \frac{t}{T_{\rm sw}}\right) \left[\, \boldsymbol{\phi}^T B_{start,ij}\, \boldsymbol{\phi} - \boldsymbol{\phi}^T\, \boldsymbol{V}_{\rm start}\, \right]. \end{aligned} \tag{B1}$$

Our goal consists in making $T_{\rm sw}$ short enough so that the state remains almost unperturbed. Since we are only interested in the total energy, it suffices for us to verify that the Heisenberg equations for $\phi_j\,(t)$ and $q_j\,(t)$ are as close to stationary as possible.

In order to give a proper scale for the proximity of observables and states, we group the canonical operators

$$\boldsymbol{R}^T = (X_1, \ldots, X_N, P_1, \ldots, P_N)\,, \tag{B2}$$

defined by

$$\boldsymbol{\phi} = C^{-1/2}\, \boldsymbol{X}\,, \quad \boldsymbol{q} = C^{1/2}\, \boldsymbol{P}\,, \tag{B3}$$

with the resulting Hamiltonian

$$H_E\,(t) = \frac{1}{2}\, \boldsymbol{R}^T D\,(t)\, \boldsymbol{R} - \boldsymbol{R}^T \boldsymbol{W}\,(t) \tag{B4}$$

$$D\,(t) = \begin{pmatrix} F\,(t) & 0 \\ 0 & \mathbb{1} \end{pmatrix},$$

$$F\,(t) = C^{-1/2} \left[\left(1 - \frac{t}{T_{\rm sw}}\right) B_{\rm start} + \frac{t}{T_{\rm sw}}\, B_{\rm end} \right] C^{-1/2},$$

$$\boldsymbol{W}\,(t) = \left(1 - \frac{t}{T_{\rm sw}}\right) C^{-1/2}\, \boldsymbol{V}_{\rm start}\,.$$

The evolution equations for the canonical variables become

$$\frac{{\rm d}\boldsymbol{R}}{{\rm d}t} = J\, [D\,(t)\ \boldsymbol{R} + \boldsymbol{W}\,(t)]\,, \tag{B5}$$

where J is the matrix of commutators $J_{jk} = [R_j, R_k]$

$$J = \begin{pmatrix} 0 & i\mathbb{1} \\ -i\mathbb{1} & 0 \end{pmatrix}. \tag{B6}$$

Our goal is to ensure that $\boldsymbol{R}\,(T) - \boldsymbol{R}\,(0)$ is as small as possible. More precisely, we will ensure the following:

Proposition 2. *In our protocol, let us denote by Ω_{max} the largest frequency of the initial or final oscillator configuration. Then, if we switch couplings and frequencies over a time*

$$T_{sw} = \epsilon \times \mathcal{O}\left(\min\left\{ \frac{1}{\Omega_{max}}, \frac{2}{\|C^{-1/2}\, \boldsymbol{V}_{start}\|} \right\} \right), \tag{B7}$$

then we can ensure that the canonical observables only suffer small corrections

$$\boldsymbol{R}(T_{sw}) \sim \boldsymbol{R}_{sw}\,(0) \times [1 + \mathcal{O}\,(\epsilon)] + \mathcal{O}(\epsilon). \tag{B8}$$

Proof. The formal solution to the Heisenberg dynamics of our observables is given by

$$\boldsymbol{R}\,(T) = U\,(T, 0)\, \boldsymbol{R}\,(0) + \int_0^T {\rm d}t\, U\,(T, t)\, \boldsymbol{W}\,(t)\,, \tag{B9}$$

with the orthogonal operator given by

$$\frac{\rm d}{{\rm d}t}\, U\,(t, t_0) = J\, D\,(t)\, U\,(t, t_0)\,, \quad U\,(t_0, t_0) = \mathbb{1}\,. \tag{B10}$$

The second term in Eq. B9, which we call $\boldsymbol{R}_{\rm drive}$, can be easily bounded by

$$\|\boldsymbol{R}_{\rm drive}\| \leq \frac{T_{\rm sw}}{2} \left\| C^{-1/2}\, \boldsymbol{V}_{\rm start} \right\|, \tag{B11}$$

from which it is obtained that

$$T_{\rm sw} = \mathcal{O}\left(\frac{2\epsilon}{\left\| C^{-1/2}\, \boldsymbol{V}_{\rm start} \right\|} \right) \ \Rightarrow\ \|\boldsymbol{R}_{\rm drive}\| = \mathcal{O}\,(\epsilon)\,. \tag{B12}$$

We focus now on $U(t)$ and on how it deviates from the identity. Our bound for this term relies on the Magnus expansion of the time evolution orthogonal operator

$$U(t,0) = e^{\Omega(t,0)}, \tag{B13}$$

The matrix function $\Omega(t,0)$ is constructed as a series expansion $\Omega(t,0) = \sum_j \Omega_j(t,0)$, which receives the name of Magnus expansion. The contributions to this series are obtained recursively from the first term $\Omega_1(t,0) = \int_0^t \mathrm{d}\tau\, B(\tau)$. The Magnus expansion for $\Omega(t,0)$ is absolutely convergent [27] if

$$\int_0^t \mathrm{d}\tau \left\| J\, D(\tau) \right\| < \frac{1}{2}\int_0^{2\pi} \mathrm{d}x \left(2 + \frac{x}{2}\left(1 - \cot\frac{x}{2}\right)\right)^{-1}, \tag{B14}$$

where the rhs integral of (B14) is to be computed numerically. For the particular switching profile (B4), this bound can be approximated as

$$T_{\mathrm{sw}}\, \frac{\left\| J\, D(0) \right\| + \left\| J\, D(T_{\mathrm{sw}}) \right\|}{2} < 1\,. \tag{B15}$$

We can now use the fact that $\|J\, D\| = \|D\|$ and that the spectrum of $D(t)$ gives us the instantaneous eigenfrequencies of the harmonic oscillator array, Ω_n. We may thus write

$$T_{\mathrm{sw}} \max\left\{\Omega_n^{(0)}, \Omega_n^{(f)}\right\} =: T_{\mathrm{sw}}\, \Omega_{\max} < 1\,, \tag{B16}$$

using the eigenfrequencies of the initial and final problem. If this bound is satisfied, the Magnus expansion may be truncated at first order to estimate that the time evolution during the quenching window differs from the identity as

$$\left\| U(T_{\mathrm{sw}}) - \mathbb{I} \right\| \leq \mathcal{O}\left(T_{sw}\Omega_{\max}\right). \tag{B17}$$

The condition for a good fidelity follows from (B17):

$$T_{\mathrm{sw}} = \epsilon \times \mathcal{O}\left(\frac{2}{\Omega_{\max}}\right). \tag{B18}$$

□

This criterion is sufficient to guarantee that the evolution during the switching time does not significantly alter the final energy of the quenched state. If the initial state is Gaussian, which is the case for the ground state of the oscillator or any thermal state, its evolution under the quench Hamiltonian will preserve this property. We also know that Gaussian states are fully characterized by the first and second moments of the canonical operators,

$$\boldsymbol{r}(t) := \langle \boldsymbol{R}(t) \rangle\,, \quad \Gamma_{jk}(t) := \langle \{R_j(t), R_k(t)\} \rangle\,. \tag{B19}$$

Any other expectation value, including the energy and the fidelity of the state to the ideal reference, can be computed using these quantities. The bounds from Proposition 2 imply that all moments are well approximated by our choice of quench times

$$\boldsymbol{r}(T_{\mathrm{sw}}) = \boldsymbol{r}_{\mathrm{ideal}} + \mathcal{O}(\epsilon)\,, \tag{B20}$$

$$\Gamma(T_{\mathrm{sw}}) = \Gamma_{\mathrm{ideal}} + \mathcal{O}(\epsilon)\,. \tag{B21}$$

We, therefore, conclude that the final energy, the final energy distribution or other properties will be well approximated after the quench, as stated in Proposition 2.

Appendix C: Alternative measurement schemes

In the main body of the manuscript we described how it would suffice to measure the total energy that leaks out of the resonators and how this provides already information about the Franck-Condon profile. In practical situations this possibility might be hindered by noise in the amplifiers, or a limited bandwidth of them. In this section provide other alternative measurement schemes that build on existing developments in circuit-QED to provide three more interrogation schemes for our emulator.

a. Photon counting

Alternatively, we can instead measure the number of photons in each resonator and reconstruct the observable

$$E = \sum_j \hbar\omega_j^{(\mathrm{end})}\, n_j\,. \tag{C1}$$

To measure each resonator population we may rely on the method from [28], where a qubit is coupled to the resonator and brought close to resonance. Such as setup is sketched in Fig. 2, with qubits sitting close to each of the coupled resonators. Starting with the qubit in the ground state, and bringing the frequency of the j-th qubit close to that of its neighboring j-th resonator, we will see both elements experience Rabi oscillations, which by themselves give information about the photon number population, n_j.

b. QND measurement

We can also perform a quantum non-demolition (QND) measurment of the number of photons on each of the resonators by using the ancillary qubits depicted in Fig. 2. In the dispersive regime, where qubits are far off-resonance from the resonators, qubits undergo a photon number-dependent energy splitting

$$\Omega_{n,j} = \Omega_{0,j} + (2\, n_j + 1)\, \frac{g_j^2}{\Delta_j}\,, \tag{C2}$$

where $\Omega_{0,j}$ is the bare energy gap of the j-th qubit and g_j is the coupling to the j-th resonator with detuning Δ_j. The qubits associated to the translational and rotational degrees of freedom can be post-selected by keeping them uncoupled from their respective cavities.

Driving each qubit at a different frequency $\Omega_{n,j}$, we detect a Stark shift $\xi_{0,j} = g_j^2/\Delta_j$ on the frequency ω^r of

the readout cavity [29, 30]

$$\hat{\omega}_j^r = \omega^r + \xi_{0,j} \left\langle \sigma_j^z \right\rangle , \tag{C3}$$

which depends on the qubit response to the driving field. If the driving matches the qubit frequency Ω_n, then $\left\langle \sigma_j^z \right\rangle = 0$, otherwise $\left\langle \sigma_j^z \right\rangle = -1$. By monitoring transmission in the readout cavity, we guess the number of photons n_j in the j-th tuneable resonator. When the qubit is driven at the frequency $\Omega_{n,j}$, we measure a cavity frequency $\hat{\omega}_j^r = \omega^r$, and $\hat{\omega}_j^r = \omega^r - \xi_{0,j}$ otherwise.

The maximum number of photons that can be resolved using this technique is given by $2\xi_{0,j}/\gamma_j$, where γ_j is the decay rate of the j-th tuneable resonator. Using realistic values of circuit QED experiments, we get that $n_{\max} \simeq 6$ [30]. This figure is well above the expected number of phonons that populate the vibrational modes of a molecule in spectroscopic experiments ($n_{\text{vib}} \simeq 3$) [5].

c. *Metrology with entangled states*

Finally, we could also consider a QND measurement scheme using a similar setup to the one discussed in the previous paragraphs. In this alternate method the qubits that are coupled to the cavities associated to the vibrational modes of the molecule would be prepared in the GHZ state $\frac{1}{\sqrt{2}} \left(|00\ldots0\rangle + |11\ldots1\rangle \right)$. Switching on the off-resonant coupling between the qubits and the cavities during a window of time τ introduces a photon number dependent phase factor

$$\phi = \sum_{i=1}^{N} \frac{g_i^2}{\omega_i} n_i \tag{C4}$$

in the state of the qubits, which now becomes $\frac{1}{\sqrt{2}} \left(e^{-i\phi\tau} |00\ldots0\rangle + e^{i\phi\tau} |11\ldots1\rangle \right)$. If the couplings are tuned such that they correspond to a small (but known) fraction $\chi \ll 1$ of the frequency of the mode to which each qubit is coupled $g_j = \chi\, \omega_j$ (in order to remain in the dissipative limit), then this phase becomes the total energy of the system up to the multiplicative factor χ:

$$\phi = \chi \sum_{j=1}^{N} \omega_j\, n_j = \chi E\,. \tag{C5}$$

Applying the inverse GHZ gate leads to the state

$$|\psi\rangle = \cos \chi E\tau\, |00\ldots0\rangle - i \sin \chi E\tau\, |11\ldots1\rangle\,. \tag{C6}$$

Making use of a qubit readout scheme such as the one discussed in the previous subsection, the qubit (notice that we need only to measure one of them) is found at the excited state with probability $P_1(\tau)$, as a function of the interaction time τ. This probability corresponds to the probability of the simulation finishing at a certain energy $P(E)$ through the formula

$$P_1(\tau) = \int \mathrm{d}E\, P(E) \left| \sin \chi E\tau \right|^2 , \tag{C7}$$

from which it is obtained, by applying the Fourier cosine transformation, that

$$P(E) = -\frac{4\chi}{\pi} \int_0^\infty \mathrm{d}\tau \cos 2\chi E\tau\, P_1(\tau)\,. \tag{C8}$$

By repeating many instances of the same simulation for different interaction times τ, the excitation probability $P_1(\tau)$ is obtained, from which it is possible to obtain the probability $P(E)$, directly connected to the Franck-Condon profile.

[1] P. I. Bunyk, E. Hoskinson, M. W. Johnson, E. Tolkacheva, F. Altomare, A. J. Berkley, R. Harris, J. P. Hilton, T. Lanting, and J. Whittaker, ArXiv e-prints (2014), arXiv:1401.5504 [quant-ph].

[2] R. Harris, T. Lanting, A. J. Berkley, J. Johansson, M. W. Johnson, P. Bunyk, E. Ladizinsky, N. Ladizinsky, T. Oh, and S. Han, Phys. Rev. B **80**, 052506 (2009).

[3] M. W. Johnson, P. Bunyk, F. Maibaum, E. Tolkacheva, A. J. Berkley, E. M. Chapple, R. Harris, J. Johansson, T. Lanting, I. Perminov, E. Ladizinsky, T. Oh, and G. Rose, Superconductor Science and Technology **23**, 065004 (2010).

[4] S. Boixo, T. F. Rønnow, S. V. Isakov, Z. Wang, D. Wecker, D. A. Lidar, J. M. Martinis, and M. Troyer, Nature Physics **10**, 218 (2014).

[5] J. Huh, G. G. Guerreschi, B. Peropadre, J. R. McClean, and A. Aspuru-Guzik, Nature Photonics **9**, 615 (2015), arXiv:1412.8427 [quant-ph].

[6] P. O'Malley, R. Babbush, I. Kivlichan, J. Romero, J. McClean, R. Barends, J. Kelly, P. Roushan, A. Tranter, N. Ding, *et al.*, arXiv preprint arXiv:1512.06860 (2015).

[7] A. Aspuru-Guzik, A. D. Dutoi, P. J. Love, and M. Head-Gordon, Science **309**, 1704 (2005), quant-ph/0604193.

[8] L. García-Álvarez, U. Las Heras, A. Mezzacapo, M. Sanz, E. Solano, and L. Lamata, Scientific Reports **6**, 27836 (2016), arXiv:1511.09355 [quant-ph].

[9] B. Peropadre, G. G. Guerreschi, J. Huh, and A. Aspuru-Guzik, Physical Review Letters **117**, 140505 (2016).

[10] J. Huh, M. Neff, G. Rauhut, and R. Berger, Mol. Phys. **108**, 409 (2010).

[11] B. Peropadre, A. Aspuru-Guzik, and J. J. García-Ripoll, ArXiv e-prints (2015), arXiv:1509.02703 [quant-ph].

[12] G. Ortiz, J. Dukelsky, E. Cobanera, C. Esebbag, and C. Beenakker, Phys. Rev. Lett. **113**, 267002 (2014).

[13] E. B.Wilson, J. C. Decius, , and P. C. Cross, *Molecular vibrations*, revised ed. (Dover, New York, 1980).

[14] P. W. Atkins and R. S. Friedman, *Molecular Quantum*

Mechanics, 5th ed. (Oxford University Press, Oxford, 2010).

[15] J. Huh, *Unified description of vibronic transitions with coherent states*, Ph.D. thesis (2011), http://publikationen.stub.uni-frankfurt.de/frontdoor/index/index/docId/21033.

[16] H.-C. Jankowiak, J. L. Stuber, and R. Berger, J. Chem. Phys. **127**, 234101 (2007).

[17] S. Rahimi-Keshari, A. P. Lund, and T. C. Ralph, Phys. Rev. Lett. **114**, 060501 (2015).

[18] J. Huh and M.-H. Yung, arXiv preprint arXiv:1608.03731 (2016).

[19] S. Aaronson and A. Arkhipov, Proceedings of the 43rd annual ACM symposium on Theory of computing - STOC '11 , 333 (2011).

[20] C. M. Wilson, G. Johansson, A. Pourkabirian, M. Simoen, J. R. Johansson, T. Duty, F. Nori, and P. Delsing, Nature (London) **479**, 376 (2011), arXiv:1105.4714 [quant-ph].

[21] M. Sandberg, C. M. Wilson, F. Persson, T. Bauch, G. Johansson, V. Shumeiko, T. Duty, and P. Delsing, Applied Physics Letters **92**, 203501 (2008).

[22] B. Peropadre, D. Zueco, F. Wulschner, F. Deppe, A. Marx, R. Gross, and J. J. García-Ripoll, Phys. Rev. B **87**, 134504 (2013).

[23] S. O. Valenzuela, W. D. Oliver, D. M. Berns, K. K. Berggren, L. S. Levitov, and T. P. Orlando, Science **314**, 1589 (2006), http://science.sciencemag.org/content/314/5805/1589.full.pdf.

[24] S. Boutin, C. Kraglund Andersen, J. Venkatraman, A. J. Ferris, and A. Blais, ArXiv e-prints (2016), arXiv:1609.03170 [quant-ph].

[25] M. Mariantoni, E. P. Menzel, F. Deppe, M. A. Araque Caballero, A. Baust, T. Niemczyk, E. Hoffmann, E. Solano, A. Marx, and R. Gross, Phys. Rev. Lett. **105**, 133601 (2010).

[26] E. P. Menzel, F. Deppe, M. Mariantoni, M. A. Araque Caballero, A. Baust, T. Niemczyk, E. Hoffmann, A. Marx, E. Solano, and R. Gross, Phys. Rev. Lett. **105**, 100401 (2010).

[27] S. Blanes, F. Casas, J. A. Oteo, and J. Ros, Physics Reports **470**, 151 (2009).

[28] M. Hofheinz, H. Wang, M. Ansmann, R. C. Bialczak, E. Lucero, M. Neeley, A. O'Connell, D. Sank, J. Wenner, J. M. Martinis, *et al.*, Nature **459**, 546 (2009).

[29] B. Johnson, M. Reed, A. Houck, D. Schuster, L. S. Bishop, E. Ginossar, J. Gambetta, L. DiCarlo, L. Frunzio, S. Girvin, *et al.*, Nature Physics **6**, 663 (2010).

[30] D. Schuster, A. Houck, J. Schreier, A. Wallraff, J. Gambetta, A. Blais, L. Frunzio, J. Majer, B. Johnson, M. Devoret, *et al.*, Nature **445**, 515 (2007).